



Enhancing retinal images by extracting structural information



G. Molodij^{a,b,*}, E.N. Ribak^b, M. Glanc^a, G. Chenegros^a

^a LESIA-Observatoire de Paris-Meudon, CNRS, Université Pierre et Marie Curie-Paris 06, Université Paris Diderot - Paris 07, 5 Place J.Janssen, 92190 Meudon, France

^b Department of Physics, Technion - Israel Institute of Technology, Haifa 32000, Israel

ARTICLE INFO

Article history:

Received 24 March 2013
Received in revised form
13 September 2013
Accepted 2 October 2013
Available online 22 October 2013

Keywords:

Image processing
Image quality assessment
Perceptual quality
Restoration

ABSTRACT

High-resolution imaging of the retina has significant importance for science: physics and optics, biology, and medicine. The enhancement of images with poor contrast and the detection of faint structures require objective methods for assessing perceptual image quality. Under the assumption that human visual perception is highly adapted for extracting structural information from a scene, we introduce a framework for quality assessment based on the degradation of structural information. We implemented a new processing technique on a long sequence of retinal images of subjects with normal vision. We were able to perform a precise shift-and-add at the sub-pixel level in order to resolve the structures of the size of single cells in the living human retina. Last, we quantified the restoration reliability of the distorted images using an improved quality assessment. To that purpose, we used the single image restoration method based on the ergodic principle, which has originated in solar astronomy, to deconvolve aberrations after adaptive optics compensation.

© 2013 Elsevier B.V. All rights reserved.

1. Introduction

Early detection of retinal pathologies can be performed by non-invasive observation of the retinal tissue to a cellular level. The ability to resolve micron scale structures in the retina can help better understand the biophysical and vision processes of the retina [1,2], and can provide early diagnosis of retinal diseases. Adaptive optics systems, initially developed for astronomy, can compensate for real-time dynamic aberrations of the eye in order to improve the resolution of images of the retina [3–6]. However, for improving resolution, the pupil has to be dilated, and as a consequence, primary and high-order aberrations are added to the ocular optics, resulting in a blurry image and suffering from a low signal-to-noise ratio. In many cases adaptive correction is partial [7]: the images of the eye are not yet limited by diffraction and current retinal imaging offers insufficient resolution, the reasons for which might also be saccades (rapid eye motion). There exist computational imaging algorithms that are able to superresolve sets of images [8–12]. Still, adaptive optics is not always fully successful on all patients and is not always able to reach the theoretical resolution. Thus we seek to supplement the partial

results of adaptive optics with image processing to improve the final image quality. Their interpretation is often difficult without a proper deconvolution processing.

Because of the level and complexity of the aberrations in the eye, computational imaging algorithms cannot improve the image significantly, since they are based on deconvolution of the aberration operator from the high-resolution image, but the time dependence of this operator is not trivial [13]. The proper estimation of the image quality and of the reliability of the deconvolution is certainly the most difficult task to perform. High resolution details clearly arise on images after the restoration with the higher contrast, but are these true details or numerical artifacts? The simplest and most widely used full-reference quality metric is the mean squared error, computed by averaging the squared intensity differences of distorted and reference image pixels, along with the related quantity of peak signal-to-noise ratio. These are appealing because they are simple to calculate, have clear physical meanings, and are mathematically convenient in the context of optimization. But they are not very well matched to perceive visual quality [14–16].

Objective methods for assessing perceptual image quality have traditionally attempted to quantify the visibility of errors between a distorted image and a reference image using a variety of known properties of the human visual system [17–19]. In the matter of sensation of light, we have to deal with quality as well as quantity. The 19th century studies of psychophysicists Weber [20] and Fechner [21] on the response of the human eye to light state that this response is logarithmic: that is, that the eye essentially takes the logarithm of the incoming optical signal.

* Corresponding author at: LESIA-Observatoire de Paris-Meudon, CNRS, Université Pierre et Marie Curie-Paris 06, Université Paris Diderot - Paris 07, 5 Place J. Janssen, 92190 Meudon, France. Tel.: +33 145077909; fax: +33 145077959.

E-mail addresses: guillaume.molodij@obspm.fr (G. Molodij), eribak@physics.technion.ac.il (E.N. Ribak), marie.glanc@obspm.fr (M. Glanc), guillaume.chenegros@obspm.fr (G. Chenegros).

In this paper, we present an image processing algorithm for resolution enhancement of retinal images. The novelty in the suggested method is the ability to significantly improve the resolution of an ensemble of poor quality retinal images using a quality assessment based on the degradation of structural information. A precise shift, select and add process is performed on a long sequence of retinal images, using image quality assessment based on the Weber–Fechner criterion. In order to evaluate the restoration reliability using the improved quality assessment, we applied successfully a restoration technique based on an estimation of the maximum of the Laplacian of the irradiance, in which an isotropic reference is obtained from the analysis of details inside the isoplanatic patch using the ergodic principle [22]. This deconvolution method arose in the cases of extended fields-of-view such as the Sun, where the texture does not often present punctual references to estimate the aberrations, but rather high resolution details that can be exploited for that purpose.

We recall briefly in Section 2 the theoretical background of the Weber–Fechner criterion we used to determine the image quality assessment, and to perform a precise shifting, selection, and addition. In this section, we present also some improvements of the criterion to quantify the visibility of errors between the distorted image and the reference image. Section 3 presents the result on real data and the different steps of the enhancement processing. Last, in Section 4, we discuss the application of this study in the fields of optics and imaging in astrophysics in order to improve the visualization of the retina at very high spatial resolution, and to implement methods for high-resolution retinal imaging purposes.

2. Weber–Fechner assessment

Most perceptual image quality assessment approaches proposed in the literature attempt to weight different aspects of the error signal according to their visibility, as determined by psychophysical measurements in humans or physiological measurements in animals. This approach was pioneered by Mannos and Sakrison [23]. The development of an image processing algorithm for resolution enhancement depends on our capability to assess the image quality. Under the assumption that human visual perception is highly adapted for extracting structural information from a scene, we use an alternative framework for quality assessment based on the analysis of the structural information [19]. Most images are highly structured in the sense that each pixel is dependent on its neighboring pixels. This dependence provides an information on the structure of objects in a scene. In this approach, we are more interested in comparing the structures between the corrected and the degraded images. After all, measurements of the image structural information give a better assessment of the corrugation perception than the estimation of errors between images. In our approach, the image quality assessment is then determined by the modification of the structural information. To fulfill this purpose, we propose to improve the Weber–Fechner criterion it takes into account the logarithmic sensitivity of eyes in terms of the light and the structural information in the image.

The image quality measurement has to take into account not only the absolute value between two pixels but also the mean values. Our Weber–Fechner quality criterion is Q_c , the relative distance between restored $I_r(i,j)$ and corrugated $I_c(i,j)$ pixels

$$Q_c = 20 \log_{10} \frac{\text{Max}[I_r^2(i,j)]}{\delta_d}, \quad (1)$$

with

$$\delta_d = \frac{1}{JJ} \sum_{i=0}^I \sum_{j=0}^J \frac{|I_r(i,j) - I_c(i,j)|}{I_r(i,j) + I_c(i,j)}. \quad (2)$$

This quality criterion Q_c drops to zero as the difference increases between the two images, and it tends to infinity as the two images become similar. We show below how this quality criterion was implemented on a long sequence of retinal images of subjects with normal vision to perform successfully a precise shift-select-and-add at the sub-pixel level.

Nevertheless, this quality criterion suffers a lack of sensitivity for images with poor contrast and the calibration remains difficult on the corrugated images. The quality criterion determined by Eqs. (1) and (2) is not able to quantify the restoration reliability of the distorted images. Stronger structural information can be characterized by the histogram of the corrugated image intensity, or by the strength of the gradients of the images. Using the dynamic range adjustment transformation from the raw image histogram to increase the contrast, Eq. (2) becomes

$$\delta_d = \frac{1}{JJ} \sum_{i=0}^I \sum_{j=0}^J \frac{[I_r(i,j) - I_c(i,j)]^2}{\text{histo}(i,j)}, \quad (3)$$

where $\text{histo}(i,j)$ is the affine transformation (see Appendix A).

Similarly, for the gradient structured function, Eq. (2) becomes

$$\delta_g = \frac{1}{JJ} \sum_{i=0}^I \sum_{j=0}^J [\nabla I_r(i,j) - \nabla I_c(i,j)]^2, \quad (4)$$

where the gradient is taken at half scale of the image spatial correlation.

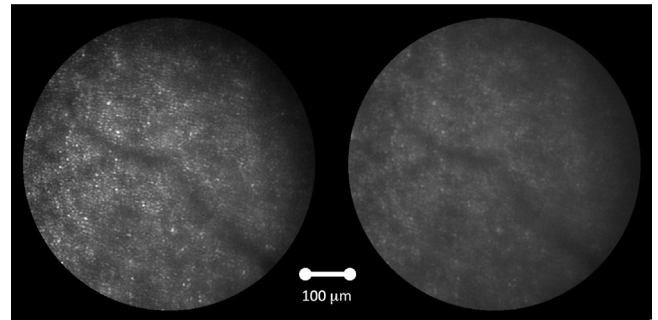


Fig. 1. Comparison between the mean processed image (left) and the best raw image (right) on data taken at the XV-XX Hospital. The r.m.s contrast value is 8.1% for the restored mean image while the value is 4.1% for the best raw image.

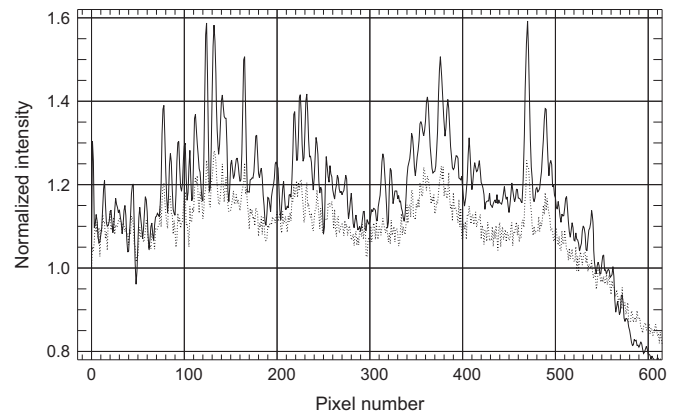


Fig. 2. Comparison of intensity profiles along the same selected lines across the retina image after the complete processing (plain line) and before the processing on the best raw image (dashed-line) of Fig. 1.

Many methods have been proposed for determining image quality, and they can be broadly classified into full-reference and no-reference methods. The full-reference methods evaluate image quality by comparing images with a reference image, which is assumed to have perfect quality. In the case of the deconvolution processing, no-reference methods can be used to assess the quality of the image. We show in Section 3.2 that the last equation leads us to a reliable estimate of the image quality after the enhancement by the deconvolution processing. We verify the linear behavior of this image quality assessment using simulation of well-known atmospheric perturbations on solar extended images and defined by a Strehl ratio. In the following, we show the different applications of the criteria defined with Eqs. (2) and (4) to respectively perform a precise shift-select-and-add at the sub-pixel level, and to quantify the restoration reliability.

3. Results

In order to test the method, we developed software in the Interactive Data Language (IDL) environment. We performed the processing method on several sets of data obtained with very different set-ups at the XV-XX Hospital and at Technion. LESIA at the Paris Observatory has invested in this technology and has constructed an optical bench with a retinal imaging adaptive optics system at the XV-XX Hospital, Paris [6,24]. The Technion invested in over-sampling large sets of retinal images use a simple

fundus camera [13]. In another version, adaptive optics is avoided by immersing the eye in saline solution, thus reducing the corneal aberrations [25]. The camera acquires multiple images of the retina, each having a low contrast. A typical comparison between a single retinal image and the final one is shown in Fig. 1 from several sequences (130 processed images) with the optical bench “OEIL” at the XV-XX Hospital. Intensity profiles before and after restoration are plotted in Fig. 2.

The proposed image processing algorithm for resolution enhancement consists of several routines which can be called in different order depending on the aim that may be to improve the image resolution, to correct the motion distortion, or to detect features with a high level of certainty, for instance. Nevertheless, the use of a multiframe mode with the shift-and-add method to increase the signal-over-noise ratio must incorporate an image selecting step. A possible evaluation to probe the reliability of the deconvolution is to repeat the processing on a set of outcomes and check the statistical apparition of the details by the structural information assessment by comparison with a randomly displayed image.

3.1. Shift-and-selection before addition

Our aim is to improve the image resolution with a high level of certainty on a selected field-of-view. This is done by dual-step accurate summation of the largest number of frames when imaging in a multiframe mode [26], instead of a single flash mode, and enabled us to use much less illumination power with greater comfort to the subjects. The novelty in the suggested method is the ability to significantly improve the resolution of an ensemble of poor quality retinal images by an evaluation of the shift correction accuracy using the structural information assessment of Eq. (2). Moreover, as a consequence of its logarithmic nature, the structural information assessment range is from 0 up to ∞ and grows smaller as the difference increases between the two images. This assessment is able to perform a precise shift-and-add at the sub-pixel level. Its range of application depends on the available structural information determined by the autocorrelation function. To save the computational resources, we proceed as follows. First, we attempt to correct the large shifts coming from the rapid eye motion using the correlation method based on the complex conjugate maximum and the fast Fourier transform algorithms. Then, we use the structural information assessment between the reference image of interest and multiple shifted images of the sequence to correct the residual. Then, we select the images according to similarity criterion, i.e., using the structural information assessment on the region of interest to select images that have been correctly shifted. Last, we sum the selected images. The accuracy of the shift-and-add method depends on the sub-field-of-view inside an isoplanatic domain. The processing reveals stochastic rotations of the field all along the retinal sequence data.

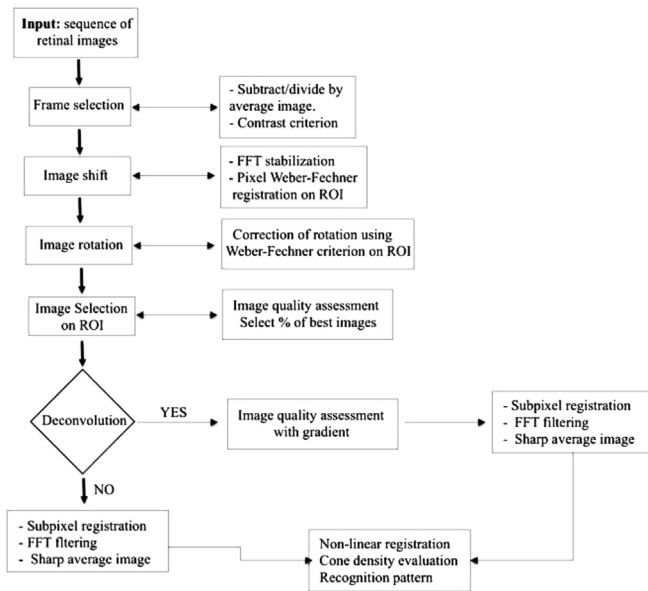


Fig. 3. Flow diagram of retinal imaging approach on the region of interest (ROI).

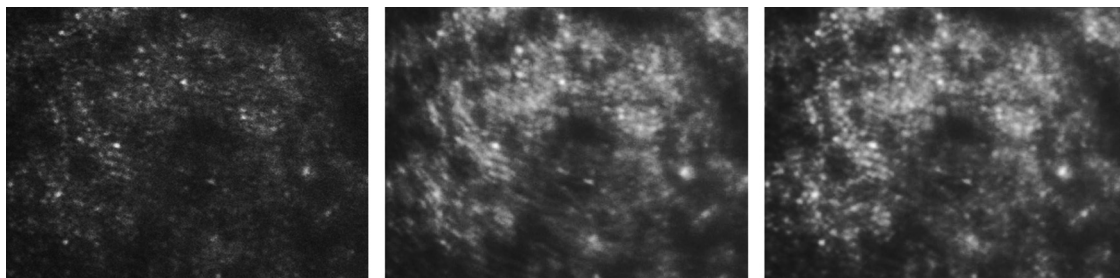


Fig. 4. Left: raw image of the retina observed on 30 January 2009 at the XV-XX Hospital. Right: the mean image (after addition) includes supplemental stage to correct adequately the rotation using the structural information assessment before addition. Middle: the mean image obtained without this supplemental correction creates a fake circular stack retina cells. The shift-and-add processing includes a selection procedure depending on the selected region-of-interest using the structural information assessment.

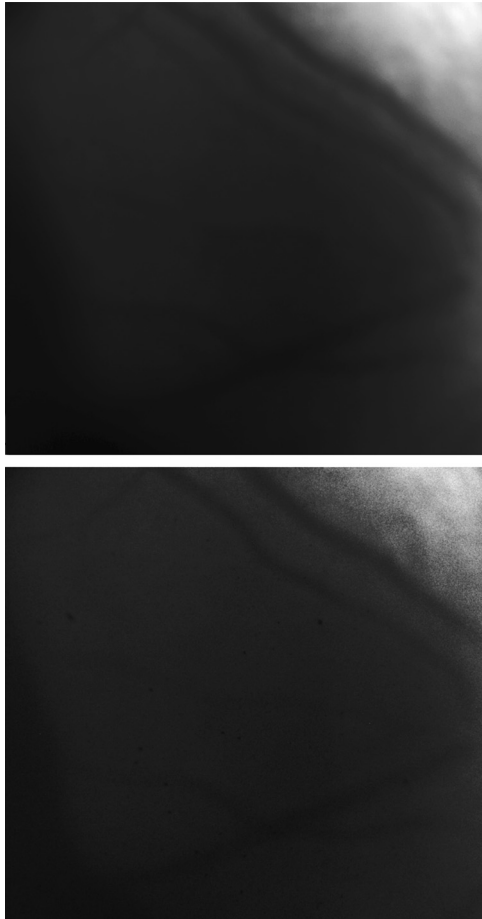


Fig. 5. (Top) final image compared to (bottom) single retinal frame. The image is 4.5° across, with its right side at 14° nasal eccentricity. Scale bar, $100 \mu\text{m}$. Final image is made up of 77 images centered at half-pixel level. Contrast values are equivalents (around 10%). By comparison, the structural information assessment gives a very high value (see Table 1).

Table 1

Image quality assessment using the r.m.s. contrast criterion (second column) and the structural information assessment 'SIA' (third column) for the two corrected images displayed (middle and right) on Fig. 4. The mean image is determined after a precise shift-and-add and image selection. The structural information assessment is calibrated from the original raw image (one pixel shift).

Retina image (s)	Contrast (%)	SIA (%)
Raw (left)	4.0	100 (ref)
Mean recentered (middle)	3.85	104
Mean recentered + rotation (right)	3.9	124

In Fig. 4 we show the supplemental stage to correct adequately the rotation using the structural information assessment before addition as indicated in the flow diagram of the Fig. 3. IDL procedure converts to polar coordinate and applies the SIA assessment as the shift method to evaluate the rotation angle on the region of interest. Two-stage image registration including correcting for rotation significantly improves the final image contrast and sharpness. The processing of mosaics seems to be indispensable to reach the high-resolution on a large field-of-view. The sharpness map of the registered and de-rotated images shows increased sharpness over most of the field of view. Then, we applied a $k-\omega$ filter to cut-off low frequencies in the Fourier domain to compensate for the intensity fluctuations [22,27]. In the Interactive Data Language (IDL) environment, the calculation time required for a current laptop is less than 1 min to perform over one hundred images for the frame selection, the registration and the deconvolution while the sub-pixel registration needs up to 20 min. To save the computational resources, we apply the sub-pixel registration only after selection of the best images.

The Technion group is producing series of data collected from retinas, barely resolving the rods and cones in order to check the efficiency of the shift and add algorithm and obtain large field-of-view to be used for diagnostic or therapeutic purposes. It developed a method to oversample these data, and use the fact that the eye keeps shifting, in order to add multiple shifted images [13]. This allows super-resolving features below the scale of the single resolution element (or camera pixel). To avoid back reflection from the cornea into the retinal camera, a wideband green LED (520 nm) was used with a central stop, forming an annular light pattern, which was focused on the pupil and crystalline lens and defocused on the retina. Fig. 5 shows the result of our processing on a relatively wide field-of-view.

3.2. Image quality assessment

An objective image quality metric can be used to dynamically monitor and adjust image quality as well as optimize algorithms and parameter settings of image processing systems. The simplest and most widely used full-reference quality metric is the image contrast, computed by

$$\left(\frac{\Delta I}{\bar{I}}\right)_{r.m.s.} = \sqrt{\frac{\sum_i^n (I_i - \bar{I})^2}{n\bar{I}^2}} \quad (5)$$

An image signal whose quality is being evaluated can be thought of as a sum of an undistorted reference signal and an error signal. A widely adopted assumption is that the loss of perceptual quality is directly related to the visibility of the error signal. The simplest implementation of this concept quantifies the strength of the error signal. But two distorted images with the same metric may have very different types of errors, some of which are much more visible than others. In Fig. 4, the two

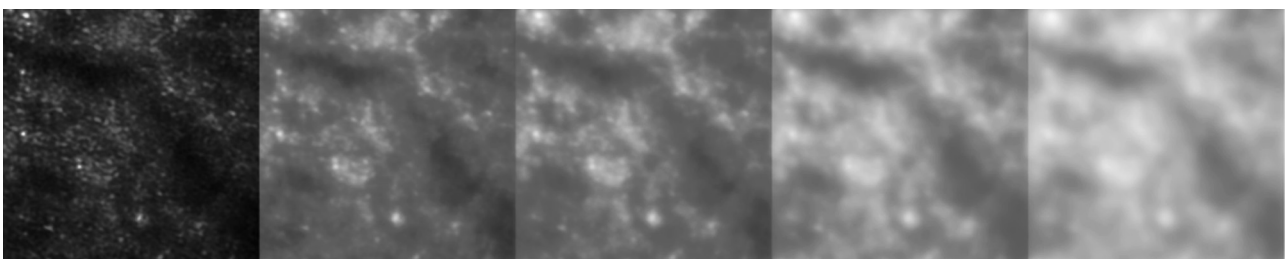


Fig. 6. Simulation of an increasing stochastic blurring determined with OTFs derived from the Zernike expansion. The retinal image left on the figure is defined as the perfect reference image associated with a Strehl value of 1.0 (perfect OTF). By comparison, the Strehl ratio of the corresponding images left to right are 0.23, 0.15, 0.065 and 0.03.

corrected images displayed (middle and right) have the same metric, i.e., an image contrast around 3.9% while the human perception distinguishes the loss of quality in the middle image. Table 1 presents a comparison between the quality assessment based on the contrast described by Eq. (5) and the structural information assessment derived from Eq. (2) on images displayed Fig. 4. By comparison, to quantify the image degradations with the structural information assessment, one considers image degradations as perceived changes in structural information. The evaluation uses the raw image in Fig. 4 (left) to calibrate the image quality degradation. A one-pixel shift corresponds to a value of 100%, for instance. Values of the assessment based on the structural information larger than 100% correspond to precise shift-and-add at the sub-pixel level.

The assessment of image quality using the structural information works well when compared to visual evaluation, although it is not well correlated with the contrast metrics. We verify this result using simulations of stochastic blurring taking into account our knowledge on the effects of the earth's atmosphere on astrophysical images. In the simulation, we estimate accurately the quality of the image using optical transfer function (OTF) convolved with the retinal images. OTFs are evaluated for a Zernike expansion following the Wang and Markey approach [28] and are applied to calculate the OTFs [29,30]. Fig. 6 shows the blurred image obtained with the corresponding calculated OTFs. Both image quality assessment using the r.m.s. contrast criterion and the structural information assessment (SIA) for the blurred images are plotted in Fig. 7. SIA criterion shows a linear behavior with respect to the determination of the Strehl ratio and yields to a more precise evaluation of the image quality assessment. The contrast criterion

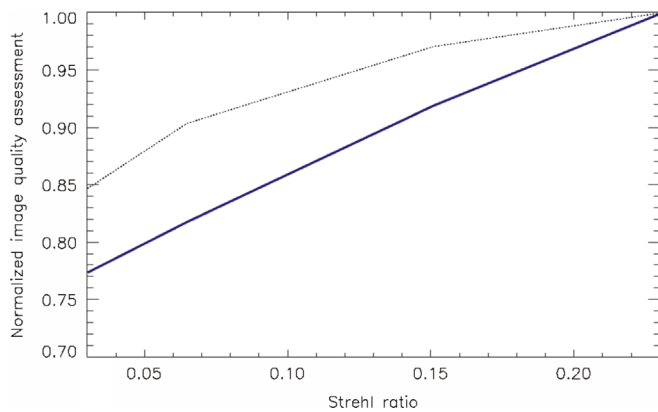


Fig. 7. Comparison of the contrast and SIA assessment image quality criteria versus the Strehl ratio derived from the simulated OTFs. The two criteria are determined on the blurred images of Fig. 6. The contrast criterion (dotted-line) shows a saturation behavior when increasing the image degradation (e.g. on small Strehl ratio) while the SIA assessment shows a linear behavior (plain line).

shows a saturation behavior for largest corrugated images as already indicated by Molodij et al. [22].

3.3. Reliability of the restoration on temporal sequences

Deconvolution is an ill-posed inverse problem that uses regularization in order to avoid an uncontrolled amplification of the noise [31]. Most deconvolution techniques boil down to the minimization (or maximization) of some criterion. The Richardson–Lucy algorithm, also known as likelihood-expectation maximization, is an iterative algorithm which converges towards the minimum of the negative log-likelihood [32]. A possible evaluation to probe the reliability of the deconvolution is to repeat the processing on a set of outcomes and check the statistical presence of the details or determine the variance. We compare the processing on each of the images separately as well as the restoration on the mean image on the entire sequence. In Fig. 8, the three corrected images displayed show a metric denied by the human perception. Table 2 presents a comparison of the quality assessment based on the contrast from Eq. (5) and the structural information assessment derived from Eq. (4) on images displayed in Fig. 8. The evaluation uses the raw image in Fig. 4 (left) to calibrate the image quality degradation. A one-pixel shift corresponds to a value of 100%, for instance. Fig. 8 shows an overcorrected image using Lucy–Richardson algorithm and simulated optical transfer function [22]. The comparison shows the lack of sensitivity of the contrast criteria to estimate the reliability of the restoration especially when considering overcompensated treatments. The difficulty to evaluate errors from global statistical analysis is due to the fact that the quality image estimator does not take into account the structural information in the image (local criteria). Fig. 9 shows the reliability of the processing on a relatively wide field-of-view observed at Technion.

4. Discussion

In this study, the purpose of retinal image registration is to align retinal images taken at different times in order to obtain a

Table 2

Image quality assessment using the r.m.s. contrast criterion (second column) and the modified structural information assessment 'MSIA' (third column) for: (left on Fig. 8) the mean deconvolved image on the sequence, (middle) the best single deconvolved image, (right) overcorrected image with simulated OTF. The mean image is determined after a precise shift-and-add and image selection. The structural information assessment is calibrated from the original raw image (one pixel shift) of Fig. 4.

Retina image(s)	Contrast (%)	MSIA distance (%)
Mean deconvolved	8.1	72.9
Single deconvolved	9.2	73.1
overcorrected	16.7	37.5

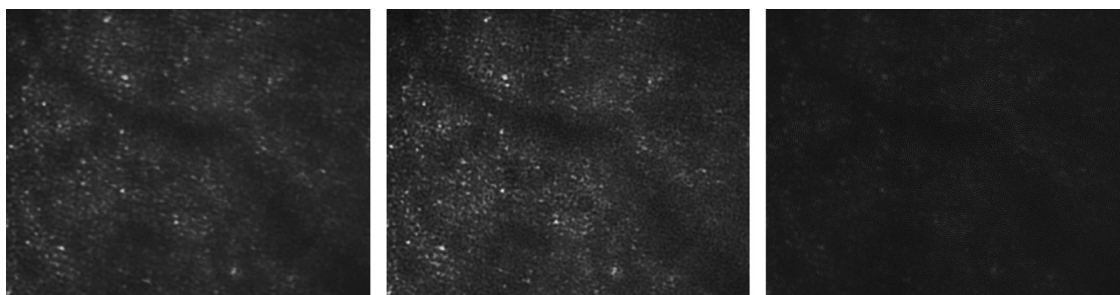


Fig. 8. Left: Mean deconvolved image of the retina at the XV-XX Hospital. Middle: One best deconvolution single image. Right: Over-correction using the simulated OTF as the deconvolution kernel.

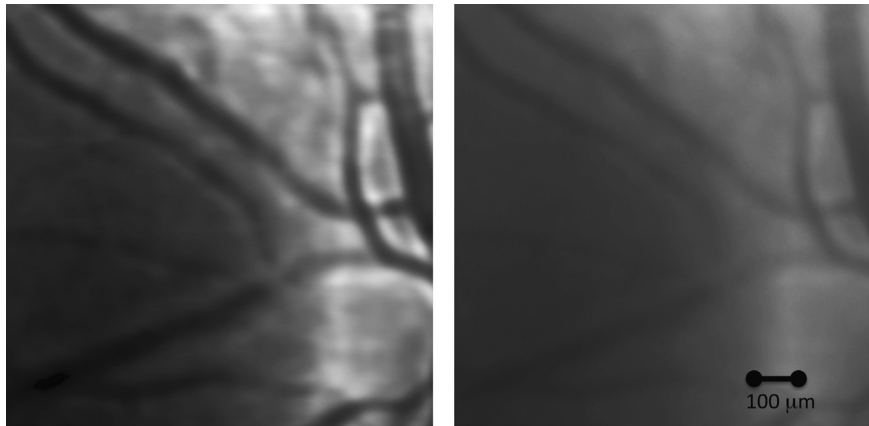


Fig. 9. Left: Deconvolution using the Ergodic principle method on a relatively wide field-of-view by comparison with the final image (right) that is made up of 77 images centered at half-pixel level. Contrast value is 1% for the deconvolved image (10% for the final image) while the structural information assessment gives a value of 80%.

very sharp and high contrast average image, after the retinal motion is corrected. We have carried out the registration to measure translation in two stages; a coarse stage followed by fine registration. Sub-pixel translation measured using the structural information is found to give good results. We have confirmed that correcting rotation of the images provides a significant improvement, especially at the edges of the image. We observed that selecting the better quality frame for image registration gives improved resolution, at the expense of the signal-to-noise. The sharpness map of the registered and de-rotated images shows increased sharpness over most of the field-of-view. The assessment of image quality using the structural information works well when compared to visual evaluation. In this study, we consider better quality images to mean sharp cone photoreceptors. Nevertheless, we show that the better contrast compared to the background is not a reliable assessment while the structural information assessment matches the human perceived image quality.

The capability to resolve single cells near the center and at peripheral areas of the retina could help better understand vision processes starting from single photoreceptor cells. We can also learn about the contribution of their spatial arrangement to the human peripheral vision [33–36]. The presented processing method can be used as a medical early detection tool with a current laptop, since it affords a simple, noninvasive, low-cost measurement at relatively low illumination power.

One of the purposes of this work is also to show the sensitivity of the proposed structural information assessment to evaluate the reliability of a deconvolution method. We used the ergodic principle method (see Appendix B) to replace ensemble statistics of a random processes with spatial statistics of a single realization, to calculate the required PSF moments by spatial averages over selected spatial intervals. This method has the great advantage of not using a priori constraint and can be applied on retinal images of subjects with abnormal retina.

There is a provoking similarity between images of solar granulation and of retinal cells, both having nearly resolved features at very low contrast, and both suffering from fast random shifts within a series of images and within the images themselves. Such a similarity calls for a shared method of investigation, which should lead to the development of novel imaging tools. We propose to apply the local correlation tracking (LCT) method [38] dedicated to the solar granulation to separate the effects of the retina irregularities from artifacts resulting from the eyes movements during the measurements. The granulation survey method [39] would be useful to evaluate the density of cones. This is the

first time, to our best knowledge, that such methods will have been applied in these two diverse fields.

5. Conclusion

Image processing and pattern recognition techniques are helpful to analyze biological images but are very difficult even for state-of-the-art image processing and pattern recognition techniques [41]. Collaboration with specialists of specific eye diseases will help to develop new techniques or to choose appropriate ones. Like medicine, research on image processing and pattern recognition continues steadily and will make further progress in accuracy, robustness, versatility, usability, and computational efficiency. Many medical diagnoses can use future image processing techniques for fully automatic image analysis, such as fundus cameras, SLOs (scanning laser ophthalmoscope) and OCTs (optical coherence tomography) of the retina. Other acquisition methods will fit other tissues, so we did not wish to limit ourselves to these specific devices. They also can use future (or even present) pattern recognition techniques for improving diagnosis. In this paper, we seek to supplement the partial results of adaptive optics with original image processing techniques to enhance the resolution of retinal images and perform a medical diagnosis for health care assistance. In this work, we demonstrated a processing method that enables resolution enhancement of retinal images. The efficiency of this method has been demonstrated on an adaptive optics system as well as a rather simple optical setup without active correction of monochromatic aberrations. At this stage of the project, an analysis of a pathological database to provide reliable medical diagnostic algorithms will be necessary. This means working on images at the limit of resolution close to observation conditions with patients showing pathologies.

Acknowledgments

We would like to thank Nizan Meitav for supplying us with the wide field-of-view images at the Technion. We wish to thank particularly the referees for the accurate review of the paper, and for providing constructive comments.

Appendix A. Dynamic range adjustment transformation

In order to increase the image contrast, we applied a dynamic adjustment reframing from the histogram distribution to change

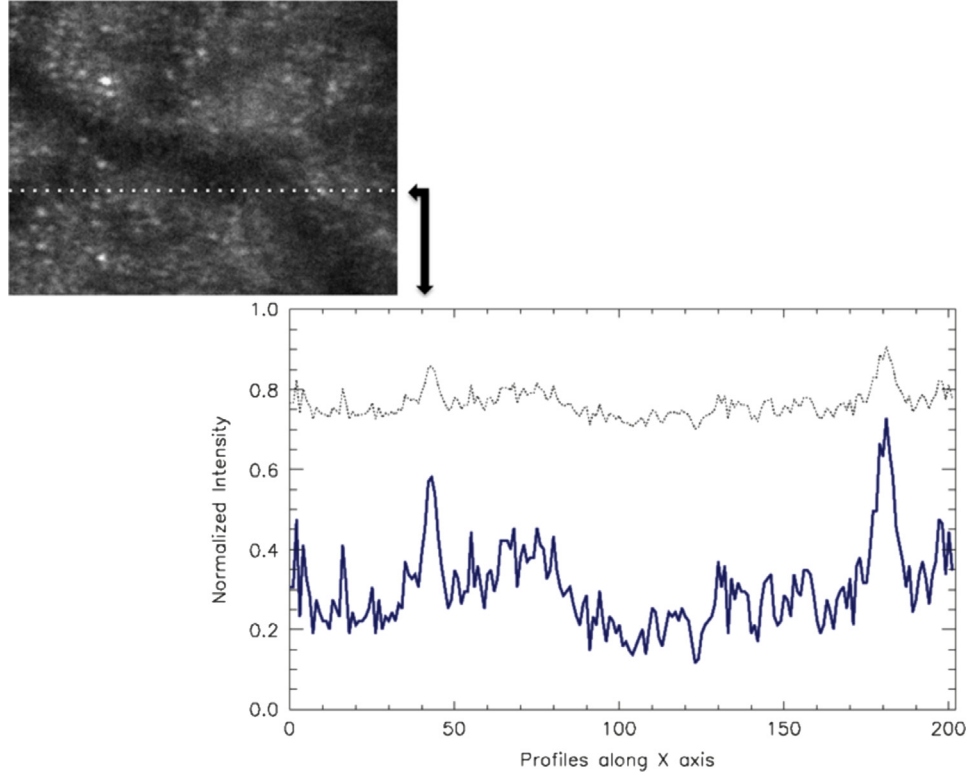


Fig. A1. Dynamic range adjustment transformation on the retinal image. The dotted line across the raw image provides a profile shown below. The plain line shows a better dynamic range after the transformation.

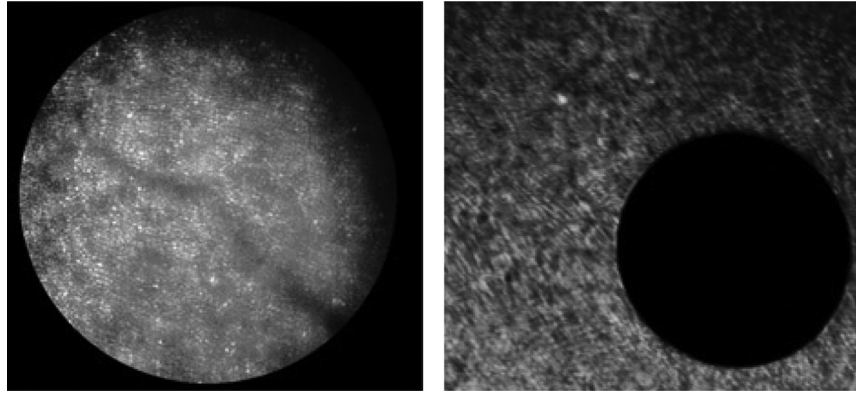


Fig. B1. On the right, the solar granulation observed on 8 June 2004 at La Tour Solaire de l'Observatoire de Paris-Meudon, in the G band, during the transit of Venus (the diameter of Venus is 21 arcsec on sky). On the left, the retina taken at the optical bench "OEIL" at the XV-XX Hospital on 30 January 2009.

the dynamic of the gray levels. In the image transformation, the gray level of the original image corresponds to a new level in the transformed image for which each pixel is treated according to its value. The reframing consists of extending the gray dynamic range denoting that the transformed image $\text{histo}(i, j)$ is an affine transformation of the raw image $\text{ima}(i, j)$,

$$\text{histo}(i, j) = a_{\text{lin}} * \text{ima}(i, j) + b_{\text{lin}}, \quad (\text{A.1})$$

with the linear coefficients:

$$a_{\text{lin}} = \frac{x_{\text{max}} - x_{\text{min}}}{I_{\text{max}} - I_{\text{min}}}, \quad (\text{A.2})$$

$$b_{\text{lin}} = \frac{1}{2} \left[x_{\text{max}} + x_{\text{min}} - \frac{I_{\text{max}} + I_{\text{min}}}{I_{\text{max}} - I_{\text{min}}} (x_{\text{max}} - x_{\text{min}}) \right],$$

I_{max} being the maximum of the intensity at x_{max} , and I_{min} the minimum of the intensity at x_{min} of the image histogram. Fig. A1 displays two profile cuts before and after the transformation.

Appendix B. Ergodic principle assumption for retinal imaging

Fig. B1 shows a great similarity between images of solar granulation and of retinal cells. We propose a novel approach to enhance the retinal imaging from the experience gained in the treatment of extended field observations of the solar surface [22]. The Ergodic principle method is able to correct the effects of atmospheric turbulence as well as static optical aberrations. Alternatively, after compensation by an adaptive optics system using a single image, it permits extraction of both object and point spread functions (PSF) within the isoplanatic patch. With current detectors, aberrations change significantly on time scales of a hundredth of a second, i.e., from one short exposure to the next. Because of ergodicity, the successive PSFs can be viewed in terms of successive stochastic events which can be characterized by a mean temporal function equal to the mean spatial function. In the case of an incoherent source with a large extent compared to the

size of the defocused PSF, it is perfectly possible to separate the perturbations from the features in the source itself [40]. The irradiance changes of the transport equation in the focal plane of an imaging system can be expressed in terms of the cross-axis derivatives of the object and moments of the PSF. Most of the contribution to the ensemble average is due to positions where the values of the derivative of the irradiance are high. So, rather than processing a statistical set of objects, it is adequate to select independently a few locations in the sensed target where the value of the Laplacian is high. Applying the Ergodic principle, the ensemble statistics of random processes is being replaced with spatial statistics of a single realization.

When observing a complex extended object, the illumination patterns show structures arising from astronomical objects mixed with variable PSFs due to atmospheric turbulence. In the speckle technique introduced by Labeyrie [42], the turbulence effects are estimated by mean of a temporal sequence analysis of the astronomical source frames. For extended sources like the Sun, the difficulty arises because each part of the object has been convolved with different point spread functions. We derived a mean spatial isotropic reference composed of different structures of the irradiance coming from the same isoplanatic domain, and calculated the required PSF moments by spatial averages over selected spatial intervals. The selected intervals are those where the object's Laplacian is large, that is, where the object has high contrast. We applied successfully the method to retinal images that allows to estimate the object with a Richardson–Lucy algorithm [43,44], based only on the single image. This statistical method is well suited to random patterns and requires only one frame and little computational resources. A way of investigation to improve the resolution of the images of the retina, used by the Technion, was a time series analysis for structural characteristics of the retina [13,37] while 3D blind deconvolution methods have been developed in France [45]. We envision a comparison in a future work with the Myopic deconvolution method on the same data [45–47].

References

- [1] K.Y. Li, A. Roorda, *J. Opt. Soc. Am. A.* 24 (2007) 1358.
- [2] Y.P. Chui, H. Song, S.A. Burns, *J. Opt. Soc. Am. A.* 25 (2008) 3021.
- [3] D. Miller, D. Williams, G. Morris, J. Liang, *Vis. Res.* 36 (1996) 1067.
- [4] J. Liang, D.R. Williams, D.T. Miller, *J. Opt. Soc. Am. A.* 14 (1997) 2884.
- [5] W. Drexler, U. Morgner, R. Ghanta, F. Kartner, J. Schuman, J. Fujimoto, *Nat. Med.* 4 (2001) 502.
- [6] M. Glanc, *Applications ophtalmologiques de l'optique adaptative* (Ph.D. thesis), Université Paris XI, 2002.
- [7] M.C. Roggemann, *Appl. Opt.* 30 (1991) 4227.
- [8] N. Nguyen, P. Milanfar, G. Golub, *IEEE Trans. Image Process.* 10 (2001) 573.
- [9] M. Elad, Y.H. Or, *IEEE Trans. Image Process.* 10 (2001) 1187.
- [10] D. Catlin, C. Dainty, *J. Opt. Soc. Am. A.* 19 (2002) 1515.
- [11] S. Farsiu, D. Robinson, M. Elad, P. Milanfar, *Int. J. Imaging Syst. Technol.* 14 (2004) 47.
- [12] J.C. Christou, A. Roorda, D.R. Williams, *J. Opt. Soc. Am. A.* 21 (2004) 1393.
- [13] N. Meitav, E.N. Ribak, *J. Opt. Soc. Am. A.* 28 (7) (2011) 1395.
- [14] B. Girod, in: A.B. Watson (Ed.), *Digital Images and Human Vision*, The MIT Press, 1993, p. 207.
- [15] P.C. Teo, D.J. Heeger, *Proc. SPIE* 2179 (1994) 127.
- [16] A.M. Eskicioglu, P.S. Fisher, *IEEE Trans. Commun.* 43 (1995) 2959.
- [17] J.M. Foley, G.M. Boynton, in: Teri B. Lawton (Ed.), *Computational Vision Based on Neurobiology*, Proceedings of SPIE, vol. 2054, 1994, pp. 32–42.
- [18] D.R. Fuhrmann, J.A. Baro, J.R. Cox, *J. Electron. Imaging* 4 (1995) 397.
- [19] Z. Wang, A.C. Bovik, H.R. Sheikh, E.P. Simoncelli, *IEEE Trans. Image Process.* 13 (4) (2004) 600.
- [20] E.H. Weber, in *Annotationes Anatomicae et Physiologicae*, Koehler, Germany, Leipzig, 1834.
- [21] G.T. Fechner, *Elemente Der Physiologischen Psychologie* (1870).
- [22] G. Molodij, S. Keil, T. Roudier, N. Meunier, S. Rondi, *J. Opt. Soc. Am. A.* 27 (11) (2010) 1459.
- [23] J.L. Mannos, D.J. Sakrison, *IEEE Trans. Inf. Theory* 4 (1974) 525.
- [24] M. Glanc, E. Gendron, F. Lacombe, D. Lafaille, J.F. Le Gargasson, P. Léna, *Opt. Comm.* 230 (4–6) (2004) 225.
- [25] N. Meitav, E.N. Ribak, A.V. Goncharov, *Opt. Lett.* 38 (2013) 745.
- [26] E.N. Ribak, *J. Opt. Soc. Am. A.* 3 (1986) 2069.
- [27] A.M. Tittle, T.D. Tarbell, K.P. Topka, S.H. Ferguson, R.A. Shine, SOUP Team, *Astrophys. J.* 336 (1989) 475.
- [28] J.Y. Wang, J.K. Markey, *J. Opt. Soc. Am. A.* 68 (1978) 78.
- [29] G. Molodij, J. Rayrole, *Astron. Astrophys. Suppl. Ser.* 128 (1998) 229.
- [30] G. Molodij, G. Aulanier, *Sol. Phys.* 276 (2012) 451.
- [31] G. Demoment, *IEEE Trans. Acoust. Speech Signal Process.* 37 (1989) 2024.
- [32] W.H. Richardson, *J. Opt. Soc. Am. A.* 62 (1972) 55.
- [33] D.R. Williams, N.J. Coletta, *J. Opt. Soc. Am. A.* 4 (1987) 1514.
- [34] D.R. Williams, *Vision Res.* 28 (1988) 433.
- [35] A.M. Labin, E.N. Ribak, *Phys. Rev. Lett.* 104 (2010) 15.
- [36] N. Meitav, E.N. Ribak, *Appl. Phys. Lett.* 99 (2011) 221910.
- [37] N. Meitav, E.N. Ribak, *Opt. Lett.* 37 (9) (2012) 1466.
- [38] L.J. November, *Appl. Opt.* 25 (1986) 392.
- [39] T. Roudier, F. Lignières, M. Rieutord, P.N. Brandt, J.M. Malherbe, *Astron. Astrophys.* 409 (2003) 299.
- [40] G. Molodij, F. Roddier, R. Kupke, D.L. Mickey, *Sol. Phys.* 206 (2002) 189.
- [41] S. Uchida, *Develop. Growth Differ.* 55 (2013) 523.
- [42] A. Labeyrie, *Astron. Astrophys.* 6 (1970) 85.
- [43] H.M. Adorf, M.J. Oldfield, in: Diana M. Worrall, Chris Biemesderfer, Jeannette Barnes (Eds.), *A.S.P. Conference Series, Astronomical Data Analysis Software and Systems I*, 1992, pp. 215–225.
- [44] R. White, in: *Newsletter of STScI's Image Restoration Project*, 1993, pp. 11–23.
- [45] G. Chenegros, L.M. Mugnier, F. Lacombe, M. Glanc, *J. Opt. Soc. Am. A.* 24 (5) (2007) 1349.
- [46] L.M. Mugnier, T. Fusco, J.M. Conan, *J. Opt. Soc. Am. A.* 21 (10) (2004) 1841.
- [47] L. Blanco, L.M. Mugnier, M. Glanc, in *SPIE vol. 7904*, 2011, pp. 790412–790418.